

Tensor networks and efficient descriptions of classical data

Sirui Lu,^{1,2} Márton Kanász-Nagy,^{1,2} Ivan Kukuljan,^{1,2} and J. Ignacio Cirac^{1,2}

¹*Max-Planck-Institut für Quantenoptik, Hans-Kopfermann-Str. 1, 85748 Garching, Germany*

²*Munich Center for Quantum Science and Technology (MCQST), Schellingstr. 4, D-80799 München, Germany*

(Dated: August 17, 2021)

We investigate the potential of tensor network based machine learning methods to scale to large image and text data sets. For that, we study how the mutual information between a subregion and its complement scales with the subsystem size L , similarly to how it is done in quantum many-body physics. We find that for text, the mutual information scales as a power law L^ν with a close to volume law exponent, indicating that text cannot be efficiently described by 1D tensor networks. For images, the scaling is close to an area law, hinting at 2D tensor networks such as PEPS could have an adequate expressibility. For the numerical analysis, we introduce a mutual information estimator based on autoregressive networks, and we also use convolutional neural networks in a neural estimator method.

I. INTRODUCTION

In the last decade, deep learning [1, 2] has taken the machine learning community by storm, achieving unprecedented accuracy in text and image classification [3, 4], generation [5–7], unsupervised learning [8] and reinforcement learning [9]. Despite these breakthroughs in applications, the theory behind deep learning based on information theory [10–15], statistical mechanics [16] and renormalization [17–20] is still being developed. A crucial question is how neural networks are capable of capturing the relevant corners of the phase space where natural image and text data resides [10, 21].

In quantum physics, the situation is quite different. A natural representation of quantum data in that fields is in terms of tensor networks, with a well-developed theory based on the entanglement [22] and mutual information (MI) [23]. Similar to how neural networks can capture the fraction of the phase space spanned by natural images and text, tensor networks arise as a natural way of representing low energy states of natural quantum systems [24]. Although these states are tremendously complex, they span only a small corner of the exponentially large Hilbert space. Identifying this corner is crucial to develop numerical methods [25], namely characterizing low energy states in terms of entanglement has allowed researchers to identify suitable variational quantum states. For instance, in one-dimension systems, it has been proven that the scaling of entanglement between a subsystem and the rest of the system should be matched by the entropy scaling of the TN states used; otherwise the TN approximation becomes numerically intractable [26]. This can be explained in terms of the so-called area law for the entanglement. States satisfying such a law can be efficiently represented in terms of matrix product states (MPS), a one-dimensional family of TNs, as shown in Fig. 1 (c). Also, in quantum critical systems, an MPS description requires polynomial growth of the bond dimension but with a higher degree due the critical scaling of entanglement [27]. Multilayer TNs such as the multi-scale entanglement renormaliza-

tion ansatz (MERA) [28] or tree TN structures [29], shown in Fig. 1 (c) seem to be a more adequate description, since they have the same scaling in the entanglement entropy. This understanding also allows ones to rule out certain architectures: for instance, TNs are not the right choice for out-of-equilibrium systems which develop volume law correlations over long time [26].

Recently, there has been a surge of interest in the machine learning community towards TNs due to their application in various unsupervised and supervised learning tasks [30–35], their connection to graphical models [32, 36], their successes in compressing neural networks [37, 38], and in generative modeling [34, 39–42].

In case of natural text, recent works [21, 43, 44] have studied the decay of correlations between characters and words, observing a power law. This power-law behavior is also exhibited by language models capable of generating text with long-range coherence, such as transformer models [45], whereas correlations decay exponentially in models that struggle to keep coherence through long texts, such as recurrent neural networks [44]. For long enough sentences, even long-short term memory (LSTM) [46] networks yield exponential decay of correlations, although they can capture long range correlations much better than RNNs empirically [44]. In physical systems, such algebraic scaling of correlations is characteristic of critical locally interacting systems [47]. In quantum critical models, this implies logarithmic scaling of the entanglement entropy [48–50]. Based on this analogy, it has been argued that in natural languages exhibit critical behavior [43], and one could thus expect that languages should possess critical properties of the mutual information, which arguably plays the role of entanglement in classical systems [51].

In this paper, we study the scaling of the mutual information for text and images. For natural text we find an algebraic scaling of mutual information between a subset and its complement, with an exponent ν close to one, i.e. giving at most a volume law. This suggests that traditional one-dimensional TN approaches will not be scalable to long texts. Additionally, this indicates that even though the correlations may decay as a power law,

the behavior in text is very different from critical quantum systems, since the MI does not have a logarithmic but a quasi volume scaling. We illustrate with a simple toy model that in classical probability distributions algebraic correlations do not necessarily imply logarithmic MI scaling. This model is based on a different structure than the hidden Markov tree model of Ref. 43, which was motivated by a tree-like linguistic structure underlying the observed power law correlations between characters. According to our analysis, the tree model creates logarithmic mutual information between regions of text, contradicting our observations. Our work thus shows that the requirement to reproduce both the scaling of mutual information and word-level correlations can be a powerful guide for linguistic models: they need to be able to explain how this scaling arises from linguistic structure - from grammatical rules and the meaning within sentences, and from cross-references, style, and global meaning on longer scales.

In the case of image data, we analyze the commonly used MNIST [52], Fashion-MNIST [53] and CIFAR-10 data sets [54] (see Fig. 1(b) for example images). In this case, area law scaling would indicate that the two-dimensional projected entangled pair states (PEPS) TNs [55] with a bond dimension mildly growing with system size would be an adequate representation. For quantum many-body systems, these TNs have been shown to be effective at representing two-dimensional gaped local systems, which also exhibit area law behavior [56–63]. Earlier works have studied MI scaling in the MNIST data set, with somewhat contradictory results [64–66]. Ref. 65 found indication of stronger than area law scaling, Ref. 64 did not find a clear indication of MI area law scaling in MNIST, whereas Ref. 66 found an area law in the TinyImages [67] dataset but not in MNIST. Our analysis based on different MI estimator methods shows close to area law scaling of MI for the simple MNIST data set, representing hand-written images, PEPS-like TNs are thus promising candidates for representing them [35]. However, our results on the more natural Fashion-MNIST and CIFAR-10 data set exhibit beyond area law scaling.

Mutual information estimation is an actively researched area [68–72], and many current methods suffer from scalability and stability, due to the difficulty of numerically reproducing high-dimensional probability distributions from samples. Here, we develop a MI estimator for images, based on an autoregressive network model [5], and we benchmark it against canonical k-nearest neighbor density estimation method (kNN) [69]. We also rely on a MI neural estimator (MINE) [70] method, where neural networks are used as variational functions for the estimator. Increasing the network complexity and changing from small fully connected networks to convolutional neural networks (CNN) [3] allows us to improve the estimation of mutual information systematically. Although earlier works have found MINE estimators hard to train [73], we could achieve stable results

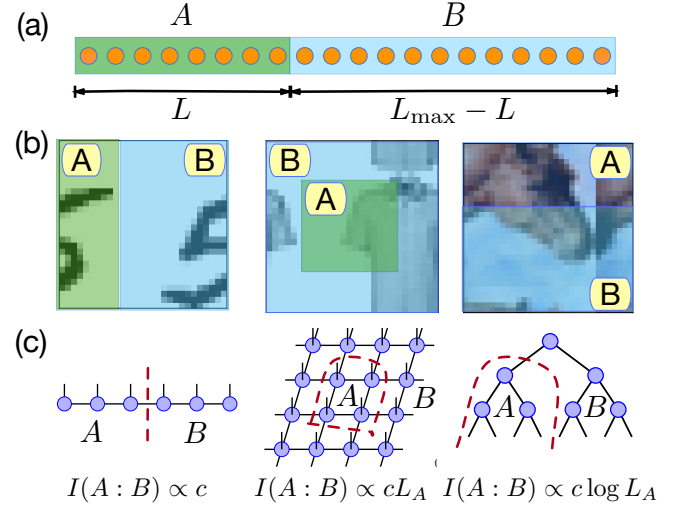


FIG. 1. (a) A schematic illustration for the partition used to define the mutual information between the two regions A and B in one-dimension. (b) In two dimensions, we consider three different partitions $A : B$, namely left : right (L : R), center : surroundings (C : S), and top : bottom (T : B). From left to right: a handwritten digit 5 (MNIST), a T-shirt (Fashion-MNIST), and a horse (CIFAR). We randomly displace the images to obtain a translationally invariant data set. (c) When the area laws hold, the mutual information $I(A : B)$ (or entanglement) is bounded by the number of sites close to the boundary, and the state has an efficient tensor network representation. We display three popular tensor network states widely used in quantum physics: matrix product states (MPS), projected entangled pairs states (PEPS), and tree tensor network states and their corresponding behaviors of the mutual information.

with them both for images and text.

This paper is organized as follows: in Sec. II, we discuss the limitations imposed by the entanglement entropy and mutual information scaling on applicability of tensor network models for describing quantum states and classical data. In Sec. III, we numerically analyze the mutual information scaling in text and images, and we introduce a toy model to understand the power-law scaling of both MI and correlations in text. Finally, we discuss the details of our numerical methods and introduce the Autoregressive-Network-based neural estimator in Sec. IV. We also discuss the mutual information neural estimation (MINE) method, where we introduce convolutional neural networks as variational functions. We also discuss a k-nearest neighbor density estimation (kNN) based method, which we use as a benchmark throughout the paper.

II. EFFICIENT DESCRIPTION OF QUANTUM SYSTEMS AND CLASSICAL DATA

A. Entanglement and quantum many-body systems

A state of a quantum many-body system on a lattice is represented by a vector in the Hilbert space of the system. A well-known fact that the dimension of Hilbert spaces grows exponentially with the lattice site is why describing quantum states is such a challenging task. In essence, the problem shares many similarities with the problem of machine learning and big data: the entire phase space is much too large to be stored in a computer's memory and processed in full completeness - one is left with the task of finding a lower-dimensional effective description of the system. In quantum mechanics, a key to that relies on the concept of entanglement entropy. Namely, it has been found that a large set of relevant quantum states lie in a special corner of the Hilbert space, the one with "low enough entanglement". The measure of that subset is much lower than that of the whole Hilbert space, enabling efficient numerical descriptions. In the following, we want to make the notion of "low enough entanglement" more precise.

A general description of a quantum state is in terms of a density matrix ρ . If we split the system into a subset A and its complement B (see Fig. 1 for an illustration), then the reduced density matrix $\rho_A = \text{tr}_B(\rho_{AB})$, a quantum counterpart of marginal distribution, is describing the state of A . For a pure state, characterized by $\text{tr}(\rho^2) = 1$, including for example ground states, the entanglement entropy (EE)

$$S(A) = -\text{tr}(\rho_A \log \rho_A) = S(B) \quad (1)$$

measures the amount of quantum entanglement between the subsystems A and B . One can then study how the EE scales with the size of the subsystem A . One of the fundamental results in quantum many-body physics is that in systems with finite correlation length, e.g., ground states of systems of massive particles, the EE only grows with the area of the region A ($S(A) \propto |\partial A|$) and not with the volume ($|A|$) [23]. This is termed the area law for entanglement and has proven for gaped 1D systems with local Hamiltonians systems [74], where an area law implies constant EE w.r.t. the partition size, and for 2D systems under few further conditions [75–77]. For certain ground states of gapless system, like free theories, critical systems, and conformal field theories (CFT), the correlation length is no longer finite, but the EE still scales slower than the volume of the subsystem, namely with a logarithmic law $S(A) \propto \log |A|$ in 1D and area law $S(A) \propto |A|$ in 2D [48–50, 78–80].

A logarithmic or area law scaling of the entanglement entropy in ground states suggests that these states only occupy a small corner of the Hilbert space. This opens up an opportunity to efficiently characterize them with a family of variational states that have the same scaling of entanglement [23, 24, 26]. Tensor networks have been

proven to be powerful representations of ground states of many-body local Hamiltonians [24]. In one dimensional systems, MPS states have area law scaling, and have been shown to be good variational states for gaped one-dimensional Hamiltonians [23]. Entanglement entropy of the multi-scale entanglement renormalization ansatz (MERA) and tree tensor networks (TTN) scales logarithmically, characteristic of quantum critical systems [28]. In higher dimensions, PEPS and MERA exhibit an area law, whereas TTNs have logarithmic scaling [24].

For one-dimensional systems, it has been proven that the states that satisfy area laws have an efficient matrix product state representation [27]; states that satisfy area laws with logarithmic corrections can also be described with MPS, although MERA and TT may be more suitable for specific models. Furthermore, algorithms based on matrix product states for ground states of 1D gaped Hamiltonians have been proved to be efficient [81]. For higher-dimensional systems, PEPS and MERA have been proven to have area laws [23], making them good candidates to describe ground states of high dimensional gaped local systems.

There are also important classes of states that do not fulfill an area law for entanglement. The first being nonequilibrium states where the EE often grows linearly in time $S(t) \propto t$ [82, 83], exceeding the available bond dimension at some point, and limiting the TN time evolution to relatively times.

B. Mutual information and classical data

The understanding gained has been that variational methods need to be able to reproduce at least as much entropy as the data we are trying to train them on. The second important class of states that generally do not satisfy an entropy area law are thermal states, which in nature are very close to classical data. In case of thermal states, which are mixed states ($\text{tr}(\rho^2) < 1$), the EE does no longer measure only the quantum entanglement but also mixedness and the thermodynamic entropy. The quantity that is well suited to characterizes the mutual dependence between the subsystems is the mutual information (MI)

$$I(A : B) = S(A) + S(B) - S(A, B), \quad (2)$$

with $S(A, B)$ denoting the entropy of the combined system of A and B and $S(A) \neq S(B)$ in general. MI has the favorable property that in both the classical and the quantum world it is an upper bound for all the correlations in the system [23], even beyond linear correlations. Both for classical and quantum systems, it has been shown that thermal states of systems with a finite range of interaction satisfy an area law MI scaling [23] and indeed it has been proven that these states can be efficiently captured using TNs [84, 85].

For classical data distributions, the entanglement en-

tropies in Eq. (2) are replaced by the Shannon entropy

$$S(A) = - \int_A \log \mathbb{P}_A \, d\mathbb{P}_A, \quad (3)$$

where \mathbb{P}_{AB} is the joint probability distribution of the statistical ensemble describing the data and $\mathbb{P}_A = \int_B d\mathbb{P}_{AB}$ is the marginal probability distribution corresponding to the subsystem A . Here, we study the scaling of mutual information in classical data to understand whether TN methods are likely to scale well for large data machine learning tasks. Based on the experience gained in the quantum realm, if a model (neural network, tensor networks, etc.) is to be expected to learn some data well, it needs to be able to produce probability distributions whose mutual information between subsystems scales least as rapidly or more as the mutual information of the data.

As illustrated in Fig. 1, we divide the system into two subsystems A and B and analyze their mutual information $I(A : B)$. In one-dimensional data such as text, we consider the left : right partition. In two-dimensional data (images), we consider two kinds of separations. The first kind is a horizontal cut that partitions the system into top : bottom (T : B) regions, where L denotes the length of the top region. The second is the center : surroundings partition (C : S), where L denotes the side of the central square.

If the area law holds, the mutual information between the two regions should be proportional to the size of the area of the interface between the two regions. For text data (1D), this would imply a MI independent of L , $I(L : R) = \text{const}$ if both A and B are large enough. For image data (2D), for T : B partitions, the size of the interface again doesn't change and we would again expect $I(T : B) = \text{const}$, while for the C : S partitions, the size of the interface grows with L , so an area law would imply $I(C : S) \sim L$. Note that for finite systems, since MI has the value 0 at the boundaries, a nonlinear growth of MI is expected before it reaches the area law plateau. In the case of volume laws, the mutual information between the two regions grows with the volume of the smaller region. This happens when each part of the system is correlated with every other part. In this case, we would observe initially (in the limit when one region is very small and the other large) in text data: $I(L : R) \sim L$ and in image data: $I(T : B) \sim L$ and $I(C : S) \sim L^2$. There could be other possible scalings of MI in between these two extreme scenarios, like logarithmic scaling $I(A : B) \sim \log(L)$ or power-law scaling $I(A : B) \sim L^\alpha$ for $0 < \alpha < 1$.

C. Machine Learning Modeling

Similar to what tensor networks is to quantum many-body states, generative neural networks try to reproduce the observed real-life distribution, for example natural images and languages. In common generative modeling

scenarios, we are given a data set consisting of M samples from the P_{data} : $D = \{\mathbf{x}_1, \dots, \mathbf{x}_M\}$, that should be approximated with a model distribution P_{model} . Here, the samples can be images, corpus, etc. After fitting the model to the samples, one can generate new samples from the learned model distribution P_{model} . The class of P_{model} is characterized by the so-called generative model. These can be divided into two categories [86]: explicit density models and implicit density models. Explicit density estimation attempts to learn the distribution $P_{\text{model}}(x)$ directly. The end result is a model that outputs the density $P_{\text{model}}(x)$ for any input x . Examples of explicit density generative models are likelihood-estimating models like probabilistic graphical models [87], autoregressive neural networks [5, 88–90] and sequence models in natural language processing [91]. Tensor networks can also be considered as a explicit density model. In machine learning community, matrix product states are commonly called Tensor Trains [92] and Tree Tensor Networks states are called Tensor Trees. Since contracting Tensor Trains and Tensor Trees can be done efficiently, they belong to tractable explicit density models. Exactly contracting a PEPS, however, is #P-COMplete in the worst case [93]. Thus, PEPS would be considered an approximate explicit density model, since approximate contractions [94] would be needed. This also makes it more difficult to directly apply PEPS as generative models in machine learning. We also mention two prominent examples of implicit density models: Boltzmann machines [95] and the generative adversarial networks [6]. Models from both classes have been applied to a wide range of problems and proven to be very successful.

III. MUTUAL INFORMATION SCALING IN CLASSICAL DATA

In this section, we analyze the mutual information scaling of both text and classical data and draw our conclusions with respect to their representational power using tensor networks. We rely on all three mutual information estimation methods discussed in Sec. IV the autoregressive network modeling estimator, the mutual information neural estimator (MINE) [70] and the k -nearest neighbor estimator (kNN) [69].

A. Power law scaling in text

Capturing the complexity of natural text by computers is the essence of the Turing test, one of the Holy Grails of computer science. The enormous complexity imposed by grammatical structure, meaning, style, and cross-references across the text make the solution of this problem notoriously hard. On the scale of sentences, grammar and meaning dictate the correlations. On the larger scale of paragraphs and even entire pieces of text, style and cross-references lead to weak but still impor-

tant correlations; hence we expect the mutual information to be high between parts of natural text. A manifestation of this is the recently observed algebraically decaying correlation on the character as well as on the word level [21, 43, 44]. This power-law behavior is also exhibited by the latest transformer language models capable of generating long coherent texts [45], whereas, correlations decay exponentially in models that struggle to keep long coherence, such as recurrent neural networks [44] and even long-short term memory (LSTM) [46] networks.

We apply the mutual information estimators to the WikiText-2 data set, consisting of 600 training articles and 2 million tokens in total. To transform words into a format understandable by computers, we use the pre-trained word-level embeddings from the 50-dimensional Glove model [96]. This representation builds a dense vector for each word while ensuring that words that often appear in a similar context, hence have similar meanings, would be close in the feature space. Hence our estimation of the mutual information takes word meaning into consideration. We have also checked that the results are robust to changing the dimensionality of the embedding space to 200.

We determine the MI using the kNN as well as the MINE estimator using both fully connected and convolutional neural networks as variational functions in the estimator, see Sec. IV. We find that both kNN and MINE methods produce almost identical results. In the case of MINE, we first used a fully-connected feed-forward neural network to serve as the score function, following the original version of Ref. 70. We find it important to use the moving average gradient trick mentioned in Ref. 70 and 97 to fix an issue that renders the optimization stable. Then, we use a text convolutional neural network [4] as the score function to further improve the mutual information neural estimator. Admittedly, this introduces some biases into the estimation, but we find that the estimated results with CNNs are larger, hence more accurate than the estimated results with feed-forward neural networks. Compared with feed-forward neural networks, CNNs also feature fewer tunable parameters, making it possible to scale up to deeper and wider networks.

In accordance with our expectations, strong connections between different pieces of the text lead to the MI scaling much steeper than critical logarithmic scaling, as shown in Fig. 2(b)-(c). In particular, we find power-law correlations for small lengths L with an exponent $\nu = 0.82(2)$ in case of the WikiText-2 data set. This scaling is thus very close to a volume law. Moreover, as indicated by the dashed line in Fig. 2(c), the scaling is very close to not only volume law scaling but that of a model in which all words are equally correlated with all others, irrespective of their distance. This would lead to a scaling of $I(L : R) \propto L(L_{\max} - L)$, which actually approximates the data well. This indicates that tensor networks may not be a suitable model for long pieces of text. As well as that, this results challenges earlier prediction by Ref. 43 that languages are characterized

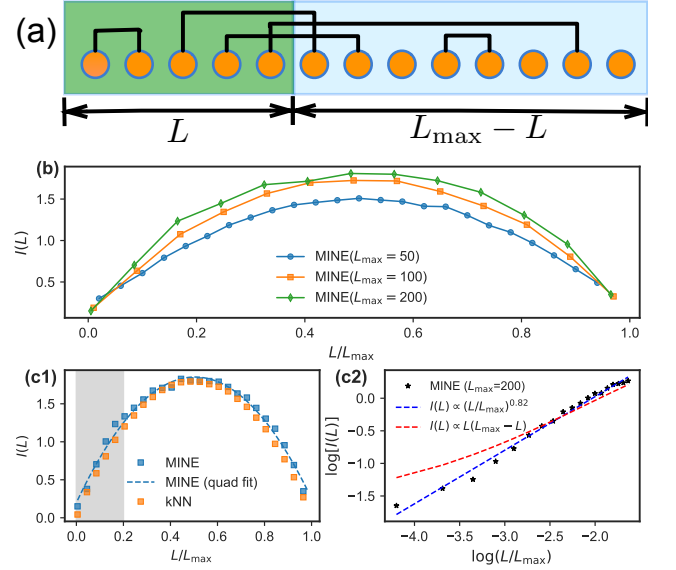


FIG. 2. (a) A schematic presentation of the random pair model. Lattice sites form maximally correlated pairs with one randomly chosen other site following a probability distribution $\rho(x - y)$. MI between two regions is given by the number of links between them. (b) MINE estimation of the MI in the WikiText-2 data set. We plot the MI between the left and the right part of the sequence, for sequence lengths 50, 100 and 200. Each word is turned into a 50-dimensional word embedding vector before being feed into the estimator. We choose the score function of the MINE as a convolutional neural network. For comparison, the MI curves $I(L : R) \propto L(L_{\max} - L)$ corresponding to an all-to-all correlated scenario is also shown (see Sec. III B). (c) kNN estimation on the WikiText-2 data set, 50-dimensional word embeddings, MaxNText=10000, K=20, for $L_{\max}=50, 100, 200$. (d) Algebraic fit of the initial part of the $I(L)$ curve (denoted with a gray area in (c)) giving $I(L/L_{\max}) \propto (L/L_{\max})^{0.82(2)}$.

by critical distributions, indicating that the structure of natural languages are rather different from local critical systems.

Besides the scaling of MI and the correlations between words, the entire distribution shows universal scaling, as shown in Fig. 2(b). As L_{\max} increases, the MI curve stays identical apart from a constant re-scaling of the overall height of the curve. This indicates that high levels of mutual information should remain characteristic even for longer texts until the point that L_{\max} reaches a new characteristic length scale of the text data, above which correlations change. Such a length scale at which correlations between individual words vanish was identified in Ref. 44. Hence, there might be that very large values of L_{\max} would lead to different scaling.

B. Model of algebraic scaling of MI and correlations

It has been observed in earlier works [21, 43] that the correlations in natural language decay algebraically, resembling critical systems in physics. In critical quantum systems, we are used to logarithmic scaling of entanglement entropy [48–50], and our observation of algebraic scaling of MI might come as a surprise at first glance. We argue here that the algebraic scaling of MI in classical data is in no way contradictory to algebraic correlation functions. The reason is that natural language data has no notion of locality which is usually imposed in quantum systems; therefore, there is a lot of freedom in terms of MI scaling. In fact, we argue that it is exactly the long-range correlation between words that leads to the algebraic scaling of MI. To illustrate this point, we discuss a simple toy example of a classical probability distribution with algebraic correlations and algebraic scaling of MI. Although motivated by the language structure, this is by no means meant to be a realistic model of natural languages. It serves merely as an example that classical probability distributions with such properties are allowed.

The model is the "random pair model", a classical cousin of the random singlet model introduced in Ref. 23. Take a probability distribution describing a 1D lattice of classical degrees of freedom, for example words in placeholders. The sites are labeled with a coordinate x . The probability distribution has the property that each site x is correlated with only a single other site y but so that the pair (x, y) shares the maximal possible amount of mutual information (see Fig. 2(a) for an illustration). The correlated pairs are distributed randomly across the lattice, following a probability distribution $\rho(x-y) = C|x-y|^{-\alpha}$ with the power $\alpha > 1$, a parameter of the model, and C a normalization constant. It is clear that this model has algebraically decaying correlation functions $\propto |x-y|^{-\alpha}$.

The MI of the model is simply given by the number of all those pairs where one member is in L and the other in R . Thus, with a simple sum $I(L : R) = \sum_{x=1}^L \sum_{y=L+1}^{\infty} \rho(x-y)$. Simplifying to extract the leading asymptotics $\rho_L(z) \equiv \sum_{w=z}^{\infty} \rho(w) \approx \frac{C}{1-\alpha}|w|^{1-\alpha}$ for $z > 0$, we have $I(L : R) = \sum_{x=1}^L \rho_L(x) \propto L^{2-\alpha}$. Therefore, this probability distribution has both algebraic correlations and algebraic scaling of MI. In fact, for $\alpha \approx 1.18$ one would recover the MI scaling observed in data. A more realistic model of natural languages would yield a different relation between the two scalings. It is easy to convince oneself by repeating the above simple calculation that for $\alpha = 2$, the model yields logarithmic MI scaling.

The random pair model is interesting also because it can give us the information of how MI scales in a finite system in a situation where every part of the system is correlated with every other part. In that case, we take that the number of correlated pairs that a fraction of the

system can form, is proportional to the volume (length in 1D) of that fraction so that the number of correlated pairs between two fractions of the system is given by the product of their volumes. This is obtained in the random pair model if one sets $\rho(x-y) = C$. In this case, the mutual information scales as $I(L : R) = |L||R| \propto L(L_{\max} - L)$ where N is the total number of lattice sites in the lattice. This curve serves as a good benchmark of how far the probability distribution of data is from such an all-to-all correlated situation.

We remark that this random pair model, although most likely does not have an efficient matrix product state representation, can be represented by restricted Boltzmann machines very easily and efficiently [98]. It would be interesting to build more sophisticated and realistic models of text in relation to the MI scaling. We leave these to future works.

C. Mutual information and entropy scaling in images

In images, correlations also arise from spatial correlations in the real world. For instance in images of faces, the presence of an eye on the left side of the image is a likely indicator that there will be another eye on the left side as well. These correlations appear on multiple scales but short-scale correlations are expected to be much more dominant than longer ones. These short-range correlations are the ones identified by the first few layers of convolutional neural networks [3]. Analysis of layer activations have indicated that local features often play the primary role in object detection tasks. Therefore, we expect the mutual information to scale closer to an area law, with additional contributions from longer range correlations.

In our analysis, we apply the Autoregressive network modeling, MINE and kNN MI estimators to low-resolution real-world image data sets, including handwritten digit images in the MNIST handwritten digit data set [52], clothing images in Fashion-MNIST[53], as well as the CIFAR data set [54] that consists of natural images of animals and means of transportation. These low-resolution data sets are widely considered to be a standard testbed for new machine learning paradigms. Since these data sets are usually focused on one object at the center, whereas the edges are more featureless, we expect only small MI contributions from the edges. This unnatural effect is not so prevalent in data sets with higher resolution images. In case of the MNIST data set of handwritten digits, the edges are completely empty, whose effect on the entropy is clearly seen in Fig. 3(a), where the slope of entropy curves at the boundary ($L \approx 0$ or $L \approx L_{\max}$) is very small. As we discuss in the Appendix A, the MI of MNIST data also drops towards the edges, since this part of the images is completely blank. Hence, in order to balance this effect, we also performed an analysis of the data where the images were made

translationally invariant by randomly shifting them, as shown in Fig. 1.

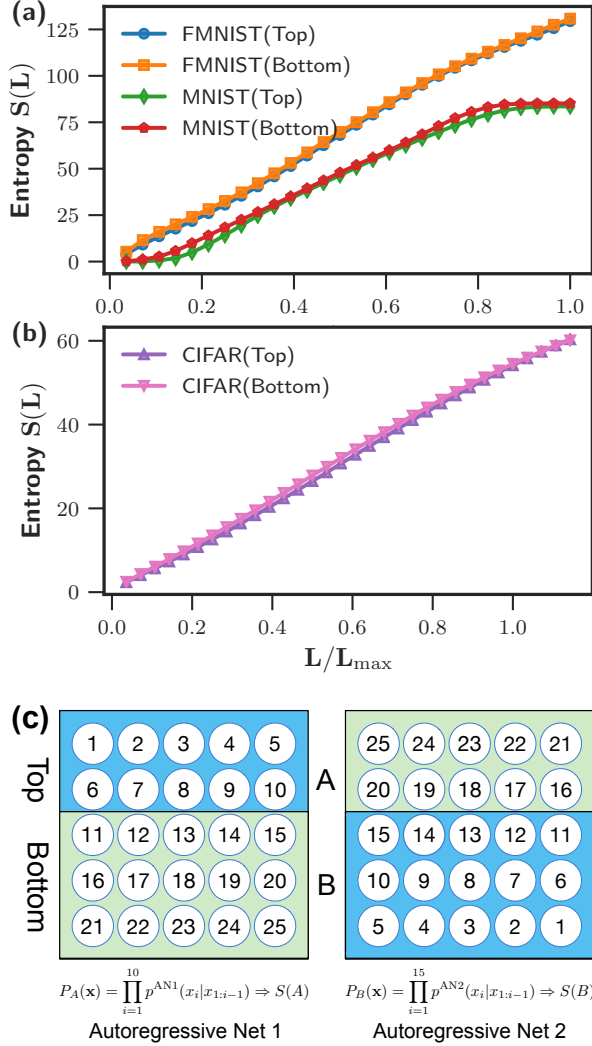


FIG. 3. Estimated Shannon entropies of subregions in image data obtained by PixelCNNs [5] and PixelCNN++ [90] trained on MNIST, Fashion MNIST (28×28), and CIFAR ($3 \times 32 \times 32$). (c) Autoregressive neural network has a sequential ordering structure: $p(\mathbf{x}) = \prod_i p(x_i | \mathbf{x}_{<i})$, meaning that the marginal distribution of the first k pixels are easy to obtain. To estimate $S(T)$ and $S(B)$ (same holds for $S(L)$ and $S(R)$), the neural networks have to be trained separately, in reverse ordering, yielding marginals of slightly different probability distributions. These plots show that they still give very similar entropy curves.

We first study the entropy of the subsystems in image data, and we find that it scales much like the thermal entropy in physical systems, exhibiting a volume law. To study entropy scaling, we use trained state-of-the-art autoregressive neural networks, as discussed in Sec. IV A, a method that is commonly used for the task. As shown in Fig. 3, a volume law in entropy is indeed in agreement with the mutual information being the right quantity to

study in image data.

In Fig. 4, we plot the observed MI curves for the $T : B$ and $C : S$ partitions on the translation-invariant MNIST data set. The mutual information $I(T : B)$ curves display a clear plateau in the central region, indicating the area law. This is well supported by the linear growth of the $I(C : S)$ curves at small values of L .

We also study more complex image data sets including FashionMNIST and CIFAR-10. Similarly, as in the case of MNIST, we randomly displace the data sets in order to make them translation invariant. The three color channels in case of CIFAR-10 increases the dimensionality of the data, posing an additional numerical challenge for estimating the MI. We use MINE and PixelCNN++ networks, and kNN methods to estimate the mutual information.

Interestingly, in these more complex data sets $I(C : S)$ still grow linearly but $I(T : B)$ never reach a plateau (Fig. 4). This suggests that in more generic images, the scaling of the MI could be faster than the area law which would then imply that TN machine learning algorithms would not scale well to large image sizes.

IV. MUTUAL INFORMATION ESTIMATORS

The MI of natural data needs to be estimated from samples, which requires modeling the distribution in a way that is independent of tensor network models. Although widely used in numerous applications [10, 99], estimating mutual information from samples remains a challenging task, especially for high dimensional data. The two families of methods traditionally used to estimate mutual information and entropy are parametric and non-parametric approaches, reviewed in Ref. 100. Early approaches mainly focused on non-parametric estimation. However, these methods often fail to give reliable results for high dimensional data. To overcome this difficulty, parametric approaches rely on a class of variational functions to estimate MI or the entropy. Recent approaches often utilize deep neural networks as variational functions. Due to the challenging nature of MI estimation, we relied here on a number of rather different methods from both families, in order to benefit from their complementary strengths and benchmark them against each other.

In this work, we develop a MI estimator based on autoregressive neural networks [88, 101–103]. We also used the popular k -nearest neighbor (kNN) estimator from the non-parametric family as a benchmark, and mutual information neural estimator (MINE) as a parametric estimator, using both fully connected and convolutional neural networks. In this section, we will introduce the essential idea of these estimators and leave the technical details of our implementations in the Appendix.

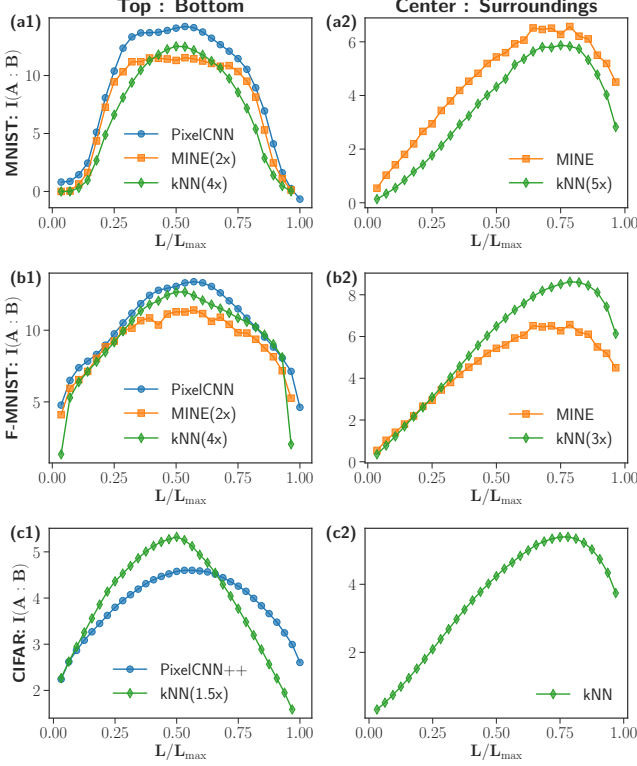


FIG. 4. Estimated mutual information scaling in image data sets. Left to Right: $I(T : B)$, $I(C : S)$. Top to Bottom: MNIST, FashionMNIST, CIFAR. For the simplest data set MNIST, we find evidence of the area law, as the $I(T : B)$ saturated in the middle and $I(C : S)$ grows linearly. For more complicated data sets (FashionMNIST and CIFAR), $I(C : S)$ still grows linearly but $I(T : B)$ does not reach a plateau, suggesting that there could be a faster than area law scaling taking place. The effect of the overall scaling factor of kNN was removed by re-scaling the results (see Appendix A).

A. Estimation from trained autoregressive networks

In generative modeling, we are given a data set \mathcal{D} of n -dimensional data points \mathbf{x} . These data points are assumed to be sampled i.i.d from the underlying distribution p_{data} . Generative modeling aims to approximate this data distribution given access to the data set \mathcal{D} . Different types of generative models are best suited for different tasks. For the convenience of estimating entropic quantities, here we consider explicit density models that provide an explicit parametric specification of the distribution of an observed random variable \mathbf{x} , specified by the log-likelihood function $\log p_{\theta}(\mathbf{x})$. Learning a generative model involves optimizing the closeness between the data and model distributions. Here, this can be done via the maximum likelihood estimation (MLE), which maximizes the log-likelihood of training data to recover the optimal model parameters: $\arg \max_{\theta \in \mathcal{M}} \frac{1}{|\mathcal{D}|} \sum_{\mathbf{x} \in \mathcal{D}} \log p_{\theta}(\mathbf{x})$.

In this section, we focus on utilizing autoregres-

sive neural networks, another tractable explicit density model, in order to estimate the entropy and MI. In general, an autoregressive model [5, 88–90] is an explicit density model that uses the chain rule to break the full probability function into products of condition probabilities: $p(\mathbf{x}) = \prod_i p(x_i | \mathbf{x}_{<i})$, where $\mathbf{x}_{<i} = [x_1, x_2, \dots, x_{i-1}]$ denotes the vector of random variables with index less than i . The conditionals are specified as parametrized functions with a fixed number of parameters. That is, we assume the conditional distributions $p(x_i | \mathbf{x}_{<i})$ to correspond to Bernoulli random variables and specified by a function (which needs to be learned) that maps $\mathbf{x}_{<i}$ to be mean of the Bernoulli distribution. Different architectures (parametrizations) have been designed for autoregressive models, including WaveNet [7], PixelRNN [5], PixelCNN [89], and PixelCNN++ [90]. These models have achieved state-of-the-art performance in many machine learning tasks.

We briefly describe how to train an autoregressive neural network. Substituting the factorized joint distribution of an autoregressive model in the maximal likelihood estimation objectives, we train the network by optimizing $\arg \max_{\theta \in \mathcal{M}} \frac{1}{|\mathcal{D}|} \sum_{\mathbf{x} \in \mathcal{D}} \sum_{i=1}^n \log p_{\theta_i}(x_i | \mathbf{x}_{<i})$ in terms of the model parameters $\theta = \{\theta_1, \theta_2, \dots\}$. After the training process, we fix the parameters of the neural networks and compute the entropy from them. Since all the conditional probabilities are normalized, calculation of the entropies of subregions that respects the sequential ordering can be done via Monte Carlo sampling. However, the mutual information is still hard to evaluate, since the sequential structure inherited in the autoregressive models forbids us from obtaining arbitrary marginal density functions. With a trained autoregressive network, we can estimate $\log p^{\text{AN1}}(x)$ and $\log p^{\text{AN1}}(x, y)$. Then we train another autoregressive network, with reversed ordering of data points, to gain access to the estimates $\log p^{\text{AN2}}(y)$ and $\log p^{\text{AN2}}(y, x)$ for points x and y in A and B , respectively, as illustrated in Fig. 3 (c). We thus estimate the mutual information as $I(A : B) = S^{\text{AN1}}(A) + S^{\text{AN2}}(B) - (S^{\text{AN1}}(A, B) + S^{\text{AN2}}(A, B)) / 2$. This is the most delicate point of this method and one needs to make sure that the distributions obtained from two different trained models are close. As shown in Fig. 3 (a), the difference between the entropies estimated from the two models at $L = L_{\text{max}}$ is negligible, indicating that two distributions are close.

Our model relies on the popular PixelCNN [89, 97] and PixelCNN++ [90] implementation [104] of density estimation to generate the conditionals $p_{\theta_i}(x_i | \mathbf{x}_{<i})$. These estimation works for top : bottom partitions, where the model can go through the image line-by-line. In the case of the center : surroundings partition, the pixels would have to be processed following a spiral path, which would be incompatible with PixelCNN or PixelCNN++ feature maps. Since the PixelCNN model assumes discrete data distribution, the pixel values were discretized dividing the color channels into 256 bins, which have been processed using the logistic mixture likelihood model introduced in the open source implementation of Ref. 104.

This discretization introduces a multiplicative factor in the mutual information estimates, as compared to the MINE and kNN models which assume continuous distributions. Hence, the results from PixelCNN and PixelCNN++ have been re-scaled in Fig. 4 by a common multiplicative factor.

B. Estimation from samples: mutual information neural estimation

Mutual information neural estimation is a popular parametric estimator, relying on neural networks that process the input data for the model. Estimation can be made more precise in a consistent manner by using more expressive networks. Besides being a benchmark for the autoregressive model for the top : bottom partition of images, we used this model extensively to handle center : surroundings partitions in images, as well as text data.

The key idea is to treat the mutual information as the KL divergence between the joint and marginal distributions and convert it into the dual representation. First, the mutual information can be expressed as the KL-divergence between the joint, \mathbb{P}_{AB} , and the product of the marginals, $\mathbb{P}_A \otimes \mathbb{P}_B$: $I(A : B) = D_{KL}(\mathbb{P}_{AB} \parallel \mathbb{P}_A \otimes \mathbb{P}_B)$, where D_{KL} is defined as $D_{KL}(\mathbb{P} \parallel \mathbb{Q}) := \mathbb{E}_{\mathbb{P}}[\log d\mathbb{P}/d\mathbb{Q}]$. Then, we use the Donsker-Varadhan dual representation of the KL divergence [105]

$$D_{KL}(\mathbb{P} \parallel \mathbb{Q}) = \sup_{T: \Omega \rightarrow \mathbb{R}} \mathbb{E}_{\mathbb{P}}[T] - \log(\mathbb{E}_{\mathbb{Q}}[e^T]), \quad (4)$$

where the supremum is taken over all functions $T : \Omega \rightarrow \mathbb{R}$ such that the two expectations are finite. It follows that

$$I_{\text{MINE}}(A, B) := \sup_{\theta \in \Theta} \mathbb{E}_{\mathbb{P}_{AB}}[T_{\theta}] - \log(\mathbb{E}_{\mathbb{P}_A \otimes \mathbb{P}_B}[e^{T_{\theta}}]). \quad (5)$$

Restricting the class of score functions T_{θ} to those represented by a class of deep neural networks θ , Eq. (5) gives rise to a lower bound on the mutual information [70]. Importantly, this lower bound is tight for the optimal score function T^* , and by increasing the expressive power of neural networks ensures that the mutual information can in principle be approximated to the desired accuracy. Being a lower bound estimator, a higher value of the MI using a different network provides a better estimation, allowing for a systematic way of improving the results. In practice, this lower bound on the mutual information is estimated on the whole data set D . The optimization task is solved by the stochastic mini-batch gradient descent. The optimized $I_{\text{MINE}}(A, B)$ can be considered as a lower bound of the true mutual information.

We note that the mutual information neural estimation of sequence data naturally fits into the framework of two-category classification. Examples include image classification and sentiment analysis of movie reviews. In these discriminative tasks, the neural network outputs a real number, which is used to indicate whether the image

is dog or cat or whether the the attitude of the movie review is positive or negative. The neural network we use to represent the score function T_{θ} defined in MINE share the same feature. In the original work of Ref. 70 the class of score functions was represented using a feed forward neural network. In this work, we are able to incorporate the most successful discriminative model, convolutional neural networks, as our score functions T_{θ} . Compared with feed-forward neural networks, CNNs are more elaborate and suitable for images [3] and texts [4], helping us to obtain better variational estimations (see Appendix B for a comparison) and scale up the calculation. Last, we remark that the mutual information neural estimator is flexible - it applies to both kinds of partitions: top : bottom and center : surroundings.

C. Estimation from samples: kNN

The k -nearest neighbor density estimator is a non-parametric approach that approximates the data distribution with one that is constant in high-dimensional simplices in space. The density $p(x)$ at point x is estimated by

$$\log \mu(x) \approx \frac{k}{M \text{Vol}_{\text{kNN}}(x)}, \quad (6)$$

where $\text{Vol}_{\text{kNN}}(x)$ is the volume of the region containing the k nearest data points to x , out of the M samples. This distribution is then used to estimate the Shannon entropy and thus the MI of data sets. The implementation [106] used in this work is based on the refined and more efficient version of this model [69]. Due to the implementation details of this algorithm, the MI is only determined up to a global multiplicative factor, that only depends on the value of k and the number of samples. Hence, we re-scaled our results up to a global factor in Fig. 4. It is expected that the kNN work well on low dimensional data, and their accuracy becomes progressively worse as the dimension of the data increases. We remark that kNN estimator can give mutual information estimation for text as well as all partitions we considered for images.

V. SUMMARY AND OUTLOOK

Our results are based on the MI analysis of natural data, making use of the deep connection between machine learning and the theory of tensor network representations in quantum many-body theory. In text data, MI scales as a power law, making commonly used MPS and tree TNs an unsuitable representation. In case of images, the handwritten MNIST data set [52], the simplest of the data sets we have investigated, has revealed a clear area law when made translation invariant. This is consistent with earlier observations that TN machine learning

algorithms classify this data set accurately [33, 35, 107]. In case of the Fashion-MNIST [53] and CIFAR [54] data sets containing more realistic images, the results are less conclusive. Whereas the center : surroundings partitions show an area law scaling, the curves for the top : bottom partitions indicate a faster than an area law scaling. The beyond area law scaling of mutual information we found suggests that more generalized tensor network states [32, 33], beyond MPS, tree TNs, or PEPS [24], should be considered for machine learning tasks. Hybrid models combining tensor networks and neural networks could also be effective [32, 35]. Any such generalized tensor network, however, must remain computationally efficient for machine learning tasks.

Our results demonstrate the effectiveness of mutual information as a theoretical tool to select, improve and rule out machine learning models, similarly to how it is used to guide development of algorithms in quantum many-body physics. There, mutual information is the key to capturing the right amount of representation power needed to characterize the small corner of the Hilbert space occupied by ground states of natural Hamiltonians. This technique could also help shed light on how neural networks are also capable of capturing natural data sets, and provide better understanding and interpretability for deep learning models.

There are many exciting possibilities for extensions of this work. From a practical point of view, it would be interesting to characterize the mutual information scaling of the distributions learnt by the state-of-the-art neural networks like the gated recurrent units [108], transformers [45], and BERT [109]. This could provide new insight into why more recent language models such as transformers [45] are capable of generating more realistic text of longer coherence than earlier models like recurrent neural nets [91] and long-short term memory networks [46]. The dynamics of mutual information within deep learning network layers have already given new insight into how these models learn and process informa-

tion [10, 110, 111]. An interesting direction would be to investigate how the mutual information between subregions in the input data evolves within neural networks as they process images or text. An equally interesting question is whether there are any other information-theoretical quantities that could help better understand how certain types of data sets occupy only a small portion of the whole parameter space and what are the characteristics that make them efficiently compressible by tensor networks or analyzable with neural networks. Research in these directions has the potential to lead to the improvement of machine learning architectures and hopefully help us towards opening the black box of neural networks.

ACKNOWLEDGMENTS

We thank Alvaro M. Alhambra and Georgios Styliaris for fruitful discussions. S.L. in addition acknowledge Yilun Yang and Dong-Ling Deng for their support and discussion. We acknowledge support from the ERC Advanced Grant QUENOCOBA under the EU Horizon 2020 program (grant agreement 742102) and from the Deutsche Forschungsgemeinschaft (DFG, German Research Foundation) under the project number 414325145 in the framework of the Austrian Science Fund (FWF): SFB F7104. I.K. is supported by the Max-Planck-Harvard Research Center for Quantum Optics (MPHQ).

Note added.—After the completion of this work, we became aware of a related study [66], focusing on the MI scaling in image data. This work finds area law scaling in the Tiny Images data set [67], but not in MNIST. We attribute the discrepancy with our work on the the fact that we made our data set translationally invariant in order to avoid the featureless outer regions of the MNIST images.

-
- [1] Y. LeCun, Y. Bengio, and G. Hinton, Deep learning, *Nature* **521**, 436 (2015).
 - [2] M. Jordan and T. Mitchell, Machine learning: Trends, perspectives, and prospects, *Science* **349**, 255 (2015).
 - [3] A. Krizhevsky, I. Sutskever, and G. E. Hinton, Imagenet classification with deep convolutional neural networks, in *Adv. Neural Inf. Process. Syst.*, Vol. 25, edited by F. Pereira, C. J. C. Burges, L. Bottou, and K. Q. Weinberger (Curran Associates, Inc., 2012).
 - [4] Y. Kim, Convolutional neural networks for sentence classification, *EMNLP 2014 - 2014 Conf. Empir. Methods Nat. Lang. Process. Proc. Conf.*, 1746 (2014), [arXiv:1408.5882](#).
 - [5] A. Van Den Oord, N. Kalchbrenner, and K. Kavukcuoglu, Pixel recurrent neural networks, in *33rd Int. Conf. Mach. Learn. ICML 2016*, Proceedings of Machine Learning Research, Vol. 48, edited by M. F. Balcan and K. Q. Weinberger (PMLR, New York, New York, USA, 2016) pp. 1747–1756.
 - [6] I. Goodfellow, J. Pouget-Abadie, M. Mirza, B. Xu, D. Warde-Farley, S. Ozair, A. Courville, and Y. Bengio, Generative adversarial nets, in *Adv. Neural Inf. Process. Syst.*, Vol. 27, edited by Z. Ghahramani, M. Welling, C. Cortes, N. D. Lawrence, and K. Q. Weinberger (Curran Associates, Inc., 2014) pp. 2672–2680.
 - [7] A. van den Oord, S. Dieleman, H. Zen, K. Simonyan, O. Vinyals, A. Graves, N. Kalchbrenner, A. Senior, and K. Kavukcuoglu, Wavenet: A generative model for raw audio (2016), [arXiv:1609.03499 \[cs.SD\]](#).
 - [8] Y. Bengio, A. Courville, and P. Vincent, Representation learning: A review and new perspectives, *IEEE Trans. Pattern Anal. Mach. Intell.* **35**, 1798 (2013), [arXiv:1206.5538](#).
 - [9] D. Silver, J. Schrittwieser, K. Simonyan, I. Antonoglou,

- A. Huang, A. Guez, T. Hubert, L. Baker, M. Lai, A. Bolton, *et al.*, Mastering the game of go without human knowledge, *Nature* **550**, 354 (2017).
- [10] N. Tishby and N. Zaslavsky, Deep learning and the information bottleneck principle, in *2015 IEEE Inf. Theory Work. ITW 2015* (Institute of Electrical and Electronics Engineers Inc., 2015).
- [11] N. Cohen, O. Sharir, and A. Shashua, On the Expressive Power of Deep Learning: A Tensor Analysis, *J. Mach. Learn. Res.* **49**, 698 (2015), [arXiv:1509.05009](#).
- [12] Y. Levine, D. Yakira, N. Cohen, and A. Shashua, Deep learning and quantum entanglement: Fundamental connections with implications to network design, in *6th Int. Conf. Learn. Represent. ICLR 2018 - Conf. Track Proc.*, 2015 (2018) [arXiv:1704.01552](#).
- [13] D.-L. Deng, X. Li, and S. Das Sarma, Quantum entanglement in neural network states, *Phys. Rev. X* **7**, 021021 (2017).
- [14] Y.-H. Zhang, Entanglement entropy of target functions for image classification and convolutional neural network (2017), [arXiv:1710.05520 \[cs.LG\]](#).
- [15] Y. Levine, O. Sharir, N. Cohen, and A. Shashua, Quantum Entanglement in Deep Learning Architectures, *Phys. Rev. Lett.* **122**, 065301 (2018), [arXiv:1803.09780](#).
- [16] Y. Bahri, J. Kadmon, J. Pennington, S. S. Schoenholz, J. Sohl-Dickstein, and S. Ganguli, Statistical mechanics of deep learning, *Annu. Rev. Condens. Matter Phys.* **11**, 501 (2020).
- [17] C. Bény, Deep learning and the renormalization group (2013), [arXiv:1301.3124 \[quant-ph\]](#).
- [18] P. Mehta and D. J. Schwab, An exact mapping between the variational renormalization group and deep learning (2014), [arXiv:1410.3831 \[stat.ML\]](#).
- [19] A. J. Gallego and R. Orus, Language design as information renormalization (2019), [arXiv:1708.01525 \[cs.CL\]](#).
- [20] M. Koch-Janusz and Z. Ringel, Mutual information, neural networks and the renormalization group, *Nat. Phys.* **14**, 578 (2018), [arXiv:1704.06279](#).
- [21] H. W. Lin, M. Tegmark, and D. Rolnick, Why Does Deep and Cheap Learning Work So Well?, *J. Stat. Phys.* **168**, 1223 (2017), [arXiv:1608.08225](#).
- [22] J. Eisert, M. Cramer, and M. B. Plenio, Colloquium: Area laws for the entanglement entropy, *Rev. Mod. Phys.* **82**, 277 (2010).
- [23] M. M. Wolf, F. Verstraete, M. B. Hastings, and J. I. Cirac, Area Laws in Quantum Systems: Mutual Information and Correlations, *Phys. Rev. Lett.* **100**, 070502 (2008).
- [24] I. Cirac, D. Perez-Garcia, N. Schuch, and F. Verstraete, Matrix product states and projected entangled pair states: Concepts, symmetries, and theorems (2020), [arXiv:2011.12127 \[quant-ph\]](#).
- [25] U. Schollwöck, The density-matrix renormalization group in the age of matrix product states, *Ann. of Phys.* **326**, 96 (2011).
- [26] N. Schuch, M. M. Wolf, F. Verstraete, and J. I. Cirac, Entropy scaling and simulability by matrix product states, *Phys. Rev. Lett.* **100**, 030504 (2008).
- [27] F. Verstraete and J. I. Cirac, Matrix product states represent ground states faithfully, *Phys. Rev. B* **73**, 094423 (2006).
- [28] G. Vidal, Class of quantum many-body states that can be efficiently simulated, *Phys. Rev. Lett.* **101**, 110501 (2008).
- [29] Y.-Y. Shi, L.-M. Duan, and G. Vidal, Classical simulation of quantum many-body systems with a tree tensor network, *Phys. Rev. A* **74**, 022320 (2006).
- [30] G. Carleo, I. Cirac, K. Cranmer, L. Daudet, M. Schuld, N. Tishby, L. Vogt-Maranto, and L. Zdeborová, Machine learning and the physical sciences, *Rev. Mod. Phys.* **91**, 045002 (2019).
- [31] S. D. Sarma, D.-L. Deng, and L.-M. Duan, Machine learning meets quantum physics, *Physics Today* **72**, 48 (2019).
- [32] I. Glasser, N. Pancotti, and J. I. Cirac, From Probabilistic Graphical Models to Generalized Tensor Networks for Supervised Learning, *IEEE Access* **8**, 68169 (2020), [arXiv:1806.05964](#).
- [33] I. Glasser, R. Sweke, N. Pancotti, J. Eisert, and J. I. Cirac, Expressive power of tensor-network factorizations for probabilistic modeling, in *Adv. Neural Inf. Process. Syst.*, Vol. 32 (Curran Associates, Inc., 2019) pp. 1498—1510, [arXiv:1907.03741](#).
- [34] E. M. Stoudenmire, Learning relevant features of data with multi-scale tensor networks, *Quantum Science and Technology* **3**, 034003 (2018).
- [35] S. Cheng, L. Wang, and P. Zhang, Supervised learning with projected entangled pair states (2020), [arXiv:2009.09932 \[cs.CV\]](#).
- [36] E. Robeva and A. Seigal, Duality of graphical models and tensor networks, *Information and Inference: A Journal of the IMA* **8**, 273 (2018).
- [37] A. Novikov, D. Podoprikin, A. Osokin, and D. Vetrov, Tensorizing neural networks, in *Adv. Neural Inf. Process. Syst.*, Vol. 28 (2015) pp. 442–450, [arXiv:1509.06569](#).
- [38] Z.-F. Gao, S. Cheng, R.-Q. He, Z. Y. Xie, H.-H. Zhao, Z.-Y. Lu, and T. Xiang, Compressing deep neural networks by matrix product operators, *Phys. Rev. Research* **2**, 023300 (2020).
- [39] Z.-Y. Han, J. Wang, H. Fan, L. Wang, and P. Zhang, Unsupervised Generative Modeling Using Matrix Product States, *Phys. Rev. X* **8**, 031012 (2018), [arXiv:1709.01662](#).
- [40] S. Efthymiou, J. Hidary, and S. Leichenauer, Tensor-network for machine learning (2019), [arXiv:1906.06329 \[cs.LG\]](#).
- [41] S. Cheng, L. Wang, T. Xiang, and P. Zhang, Tree tensor networks for generative modeling, *Phys. Rev. B* **99**, 155131 (2019), [arXiv:1901.02217](#).
- [42] J. Miller, G. Rabusseau, and J. Terilla, Tensor networks for probabilistic sequence modeling (2020), [arXiv:2003.01039 \[cs.LG\]](#).
- [43] H. W. Lin and M. Tegmark, Critical behavior in physics and probabilistic formal languages, *Entropy* **19**, 1 (2017).
- [44] H. Shen, Mutual information scaling and expressive power of sequence models (2019), [arXiv:1905.04271 \[cs.LG\]](#).
- [45] A. Vaswani, N. Shazeer, N. Parmar, J. Uszkoreit, L. Jones, A. N. Gomez, L. Kaiser, and I. Polosukhin, Attention is all you need, *Adv. Neural Inf. Process. Syst.* **30**, 5999 (2017), [arXiv:1706.03762](#).
- [46] S. Hochreiter and J. Schmidhuber, Long Short-Term Memory, *Neural Comput.* **9**, 1735 (1997).
- [47] J. Cardy, *Scaling and Renormalization in Statistical Physics*, Cambridge Lecture Notes in Physics (Cambridge University Press, 1996).

- [48] P. Calabrese and J. Cardy, Entanglement entropy and quantum field theory, *J. Stat. Mech.: Theory and Exp.* **2004**, P06002 (2004).
- [49] P. Calabrese and J. Cardy, Entanglement entropy and conformal field theory, *Journal of Physics A: Mathematical and Theoretical* **42**, 504005 (2009).
- [50] H. Casini and M. Huerta, Entanglement entropy in free quantum field theory, *Journal of Physics A: Mathematical and Theoretical* **42**, 504007 (2009).
- [51] J. Wilms, M. Troyer, and F. Verstraete, Mutual information in classical spin models, *J. Stat. Mech. Theory Exp.* **2011**, P10011 (2011), [arXiv:1011.4421](#).
- [52] Y. LeCun, C. Cortes, and C. J. C. Burges, *MNIST handwritten digit database* (1998).
- [53] H. Xiao, K. Rasul, and R. Vollgraf, Fashion-mnist: a novel image dataset for benchmarking machine learning algorithms (2017), [cs.LG/1708.07747](#).
- [54] A. Krizhevsky, V. Nair, and G. Hinton, *Cifar-10 (canadian institute for advanced research)* (2009).
- [55] F. Verstraete and J. I. Cirac, Renormalization algorithms for quantum-many body systems in two and higher dimensions (2004), [arXiv:0407066 \[cond-mat\]](#).
- [56] V. Murg, F. Verstraete, and J. I. Cirac, Variational study of hard-core bosons in a two-dimensional optical lattice using projected entangled pair states, *Phys. Rev. A* **75**, 033605 (2007).
- [57] P. Corboz, S. R. White, G. Vidal, and M. Troyer, Stripes in the two-dimensional t-J model with infinite projected entangled-pair states, *Phys. Rev. B* **84**, 041108 (2011), [arXiv:1104.5463](#).
- [58] B. Bauer, P. Corboz, A. M. Läuchli, L. Messio, K. Penc, M. Troyer, and F. Mila, Three-sublattice order in the su(3) heisenberg model on the square and triangular lattice, *Phys. Rev. B* **85**, 125116 (2012).
- [59] P. Corboz, Variational optimization with infinite projected entangled-pair states, *Phys. Rev. B* **94**, 035133 (2016).
- [60] M. Rader and A. M. Läuchli, Finite correlation length scaling in lorentz-invariant gapless ipeps wave functions, *Phys. Rev. X* **8**, 031030 (2018).
- [61] B. Ponsioen, S. S. Chung, and P. Corboz, Period 4 stripe in the extended two-dimensional Hubbard model, *Phys. Rev. B* **100**, 195141 (2019), [arXiv:1907.01909](#).
- [62] B. Vanhecke, J. Hasik, F. Verstraete, and L. Vanderstraeten, A scaling hypothesis for projected entangled-pair states (2021), [arXiv:2102.03143 \[quant-ph\]](#).
- [63] P. C. G. Vlaar and P. Corboz, Simulation of three-dimensional quantum systems with projected entangled-pair states (2021), [arXiv:2102.06715 \[cond-mat.str-el\]](#).
- [64] S. Cheng, J. Chen, and L. Wang, Information Perspective to Probabilistic Modeling: Boltzmann Machines versus Born Machines, *Entropy* **20**, 583 (2017), [arXiv:1712.04144](#).
- [65] J. Martyn, G. Vidal, C. Roberts, and S. Leichenauer, Entanglement and tensor networks for supervised image classification (2020), [arXiv:2007.06082 \[quant-ph\]](#).
- [66] I. Convy, W. Huggins, H. Liao, and K. B. Whaley, Mutual information scaling for tensor network machine learning (2021), [arXiv:2103.00105 \[quant-ph\]](#).
- [67] A. Torralba, R. Fergus, and W. T. Freeman, 80 million tiny images: A large data set for nonparametric object and scene recognition, *IEEE transactions on pattern analysis and machine intelligence* **30**, 1958 (2008).
- [68] P. Grassberger, Entropy Estimates from Insufficient Samplings (2003), [arXiv:0307138 \[physics\]](#).
- [69] A. Kraskov, H. Stögbauer, and P. Grassberger, Estimating mutual information, *Phys. Rev. E* **69**, 066138 (2004), [arXiv:0305641 \[cond-mat\]](#).
- [70] M. I. Belghazi, A. Baratin, S. Rajeswar, S. Ozair, Y. Bengio, A. Courville, and R. D. Hjelm, Mutual information neural estimation, in *35th Int. Conf. Mach. Learn. ICML 2018*, Vol. 2 (International Machine Learning Society (IMLS), 2018) pp. 864–873, [arXiv:1801.04062](#).
- [71] M. Tschannen, J. Djolonga, P. K. Rubenstein, S. Gelly, and M. Lucic, On mutual information maximization for representation learning, in *8th Int. Conf. Learn. Represent. ICLR 2020, Addis Ababa, Ethiopia, April 26-30, 2020* (OpenReview.net, 2020).
- [72] N. Carrara and J. Ernst, On the estimation of mutual information (2019), [arXiv:1910.00365 \[physics.data-an\]](#).
- [73] D. McAllester and K. Stratos, Formal limitations on the measurement of mutual information (2020), [arXiv:1811.04251 \[cs.IT\]](#).
- [74] M. B. Hastings, An area law for one-dimensional quantum systems, *J. Stat. Mech.* , P08024 (2007).
- [75] A. Anshu, I. Arad, and D. Gosset, An area law for 2d frustration-free spin systems (2021), [arXiv:2103.02492 \[quant-ph\]](#).
- [76] K. Van Acoleyen, M. Mariën, and F. Verstraete, Entanglement rates and area laws, *Phys. Rev. Lett.* **111**, 170501 (2013).
- [77] M. Mariën, K. M. R. Audenaert, K. Van Acoleyen, and F. Verstraete, Entanglement Rates and the Stability of the Area Law for the Entanglement Entropy, *Commun. Math. Phys.* **346**, 35 (2016), [arXiv:1411.0680](#).
- [78] M. Srednicki, Entropy and area, *Phys. Rev. Lett.* **71**, 666 (1993).
- [79] C. Holzhey, F. Larsen, and F. Wilczek, Geometric and renormalized entropy in conformal field theory, *Nucl. Phys. B* **424**, 443 (1994), [arXiv:9403108 \[hep-th\]](#).
- [80] G. Vidal, J. I. Latorre, E. Rico, and A. Kitaev, Entanglement in Quantum Critical Phenomena, *Phys. Rev. Lett.* **90**, 227902 (2003), [arXiv:0211074 \[quant-ph\]](#).
- [81] Z. Landau, U. Vazirani, and T. Vidick, A polynomial-time algorithm for the ground state of 1d gapped local hamiltonians (2013), [arXiv:1307.5143 \[quant-ph\]](#).
- [82] P. Calabrese and J. Cardy, Entanglement entropy and quantum field theory, *J. Stat. Mech. Theory Exp.* , 1 (2004), [arXiv:0405152 \[hep-th\]](#).
- [83] N. Schuch, M. M. Wolf, K. G. H. Vollbrecht, and J. I. Cirac, On entropy growth and the hardness of simulating time evolution, *New J. Phys.* **10**, 033032 (2008).
- [84] M. B. Hastings, Solving gapped Hamiltonians locally, *Phys. Rev. B* **73**, 085115 (2006), [arXiv:0508554 \[cond-mat\]](#).
- [85] A. Molnar, N. Schuch, F. Verstraete, and J. I. Cirac, Approximating Gibbs states of local Hamiltonians efficiently with projected entangled pair states, *Phys. Rev. B* **91**, 045138 (2015), [arXiv:1406.2973](#).
- [86] I. Goodfellow, Y. Bengio, and A. Courville, *Deep learning* (MIT press, MA, 2016).
- [87] C. M. Bishop, *Pattern recognition and machine learning* (springer, 2006).
- [88] B. Uribe, M. A. Cote, K. Gregor, I. Murray, and H. Larochelle, Neural autoregressive distribution estimation, *J. Mach. Learn. Res.* **17**, 1 (2016),

- arXiv:1605.02226.
- [89] A. Van Den Oord, N. Kalchbrenner, O. Vinyals, L. Espeholt, A. Graves, and K. Kavukcuoglu, Conditional image generation with PixelCNN decoders, in *Adv. Neural Inf. Process. Syst.* (2016) pp. 4797–4805, arXiv:1606.05328.
 - [90] T. Salimans, A. Karpathy, X. Chen, and D. P. Kingma, PixelCNN++: Improving the PixelCnn with discretized logistic mixture likelihood and other modifications, in *5th Int. Conf. Learn. Represent. ICLR 2017 - Conf. Track Proc.* (2019) arXiv:1701.05517.
 - [91] I. Sutskever, J. Martens, and G. E. Hinton, Generating text with recurrent neural networks, in *28th Int. Conf. Mach. Learn. ICML 2017, Bellevue, Washington, USA, June 28 - July 2, 2011*, edited by L. Getoor and T. Scheffer (Omnipress, 2011) pp. 1017–1024.
 - [92] I. V. Oseledets, Tensor-Train Decomposition, *SIAM J. Sci. Comput.* **33**, 2295 (2011).
 - [93] N. Schuch, M. M. Wolf, F. Verstraete, and J. I. Cirac, Computational Complexity of Projected Entangled Pair States, *Phys. Rev. Lett.* **98**, 140506 (2007).
 - [94] M. Lubasch, J. I. Cirac, and M.-C. Bañuls, Unifying projected entangled pair state contractions, *New J. Phys.* **16**, 033014 (2014), arXiv:1311.6696.
 - [95] M. Norouzi, M. Ranjbar, and G. Mori, Stacks of convolutional Restricted Boltzmann Machines for shift-invariant feature learning, in *2009 IEEE Conf. Comput. Vis. Pattern Recognit.*, 2 (IEEE, 2009) pp. 2735–2742, arXiv:1203.4416.
 - [96] J. Pennington, R. Socher, and C. Manning, Glove: Global Vectors for Word Representation, in *Proc. 2014 Conf. Empir. Methods Nat. Lang. Process.* (Association for Computational Linguistics, Stroudsburg, PA, USA, 2014) pp. 1532–1543.
 - [97] B. Poole, S. Ozair, A. Van Den Oord, A. A. Alemi, and G. Tucker, On variational bounds of mutual information, 36th Int. Conf. Mach. Learn. ICML 2019 **2019-June**, 9036 (2019), arXiv:1905.06922.
 - [98] X. Gao and L.-M. Duan, Efficient representation of quantum many-body states with deep neural networks, *Nat. Commun.* **8**, 662 (2017), arXiv:1701.05039.
 - [99] R. Devon Hjelm, K. Grewal, P. Bachman, A. Fedorov, A. Trischler, S. Lavoie-Marchildon, and Y. Bengio, Learning deep representations by mutual information estimation and maximization, *7th Int. Conf. Learn. Represent. ICLR 2019* (2019), arXiv:1808.06670.
 - [100] L. Paninski, Estimation of entropy and mutual information, *Neural Comput.* **15**, 1191 (2003).
 - [101] K. Gregor, I. Danihelka, A. Mnih, C. Blundell, and D. Wierstra, Deep autoregressive networks, in *31st Int. Conf. Mach. Learn. ICML 2014*, Vol. 4 (2014) pp. 2991–3000, arXiv:1310.8499.
 - [102] S. Reed, A. van den Oord, N. Kalchbrenner, S. G. Colmenarejo, Z. Wang, D. Belov, and N. de Freitas, Parallel multiscale autoregressive density estimation (2017), arXiv:1703.03664 [cs.CV].
 - [103] Z. Wang and E. J. Davis, Calculating Rényi entropies with neural autoregressive quantum states, *Phys. Rev. A* **102**, 062413 (2020), arXiv:2003.0135.
 - [104] (2019), see https://github.com/kamenbliznashki/pixel_models.
 - [105] M. D. Donsker and S. R. S. Varadhan, Asymptotic evaluation of certain markov process expectations for large time. IV, *Commun. Pure Appl. Math.* **36**, 183 (1983).
 - [106] (2019), see <https://github.com/gregversteeg/NPEET>.
 - [107] E. Stoudenmire and D. J. Schwab, Supervised learning with tensor networks, in *Adv. Neural Inf. Process. Syst.* **29**, edited by D. D. Lee, M. Sugiyama, U. V. Luxburg, I. Guyon, and R. Garnett (Curran Associates, Inc., 2016) pp. 4799–4807.
 - [108] J. Chung, C. Gulcehre, K. Cho, and Y. Bengio, Empirical evaluation of gated recurrent neural networks on sequence modeling (2014), arXiv:1412.3555 [cs.NE].
 - [109] J. Devlin, M.-W. Chang, K. Lee, and K. Toutanova, Bert: Pre-training of deep bidirectional transformers for language understanding (2019), arXiv:1810.04805 [cs.CL].
 - [110] N. Tishby, F. C. Pereira, and W. Bialek, The information bottleneck method (2000), arXiv:0004057 [physics].
 - [111] Z. Goldfeld, E. van den Berg, K. Greenewald, I. Melnyk, N. Nguyen, B. Kingsbury, and Y. Polyanskiy, Estimating Information Flow in Deep Neural Networks, in *36th Int. Conf. Mach. Learn. ICML 2019*, Vol. 97, edited by K. Chaudhuri and R. Salakhutdinov (PMLR, 2018) pp. 2299–2308, arXiv:1810.05728.
 - [112] N. Srivastava, G. Hinton, A. Krizhevsky, I. Sutskever, and R. Salakhutdinov, Dropout: A simple way to prevent neural networks from overfitting, *Journal of Machine Learning Research* **15**, 1929 (2014).
 - [113] D. P. Kingma and J. Ba, Adam: A method for stochastic optimization (2014), arXiv:1412.6980 [cs.LG].
 - [114] V. Nair and G. E. Hinton, Rectified linear units improve restricted boltzmann machines, in *Proc. 27th Int. Conf. Mach. Learn.*, ICML’10 (Omnipress, USA, 2010) pp. 807–814.
 - [115] A. Paszke, S. Gross, F. Massa, A. Lerer, J. Bradbury, G. Chanan, T. Killeen, Z. Lin, N. Gimelshein, L. Antiga, A. Desmaison, A. Kopf, E. Yang, Z. DeVito, M. Raison, A. Tejani, S. Chilamkurthy, B. Steiner, L. Fang, J. Bai, and S. Chintala, Pytorch: An imperative style, high-performance deep learning library, in *Adv. Neural Inf. Process. Syst.* **32**, edited by H. Wallach, H. Larochelle, A. Beygelzimer, F. d Alche-Buc, E. Fox, and R. Garnett (Curran Associates, Inc., 2019) pp. 8024–8035.

Appendix A: k -nearest neighbor estimator

We used the popular kNN estimator [69] throughout this paper to benchmark other estimators. kNN is expected to work best for small dimensional data. An important characteristic of this estimator is the overall scaling factor of its MI estimates, which depends on the number of input data points n_{data} and the parameter k of nearest neighbors used in the density estimation step (see Sec. IV). In Fig. A.1, we show kNN-based MI estimates of the MNIST data set, without making the images translationally invariant. We empirically find that the scaling only depends on the ratio k/n_{data} .

Fig. A.1 also clearly displays the effect of the blank areas towards the edges of MNIST images, as the MI decays towards the edges. Furthermore, the curves for the top:bottom partition do not feature the flat plateau observed in Fig. 4 (a), characteristic of the area law behavior in translationally invariant MNIST images. This

behavior is also due to the edges that suppress the MI values even in the vicinity of the center of the images.

Appendix B: Mutual information neural estimator

In this Appendix, we give more technical details of our implementation of the MINE estimator [70]. This model allows the flexible use of various neural networks to be used as score functions. Being a lower bound estimator, the accuracy of the MI estimation can always be improved by achieving a higher MI estimate using a more expressive score function. We compare results obtained using full connected and convolutional neural network (CNN) used both for text and images.

As mentioned in the main text, Ref. 70 chose the score function T_θ as a multi-layer fully-connected feed forward neural network (FC-FFNN). In order to use a network with more expressive power and more suitable for images and text, we choose T_θ as CNN consisting of three layers: a 3D convolution layer, a 2D maxpooling layer, a dropout [112] layer with rate 0.25, and a fully-connected flattening layer with 0.25 dropout regularization. The last layer is then connected to the final fully-connected layer with a single output. This output is the score function T_θ in Eq. (5). We choose the Adam optimizer [113] and a batch size of 128. The learning rate is set to be 10^{-4} during training. The activation function is ReLU [114].

We compare the above CNN with a FC-FFNN, which is composed of an input layer with 28×28 neurons, a hidden layer with 500 sigmoid neurons, and an analogous output layer with one sigmoid neuron. When estimating the mutual information with the FC-FFNN, we use the same optimizer, learning rate, batch size, and the number of epochs as in the case of CNNs. We implemented the mutual information neural estimation procedure using PyTorch [115].

In Fig. B.2, we compare the performances of MINE using FC-FFNN and CNN on MNIST and Fashion-MNIST data. We find that CNNs always outperform FC-FFNNs as they consistently give higher MI values. Hence we use CNN-based MINE results throughout the main text.

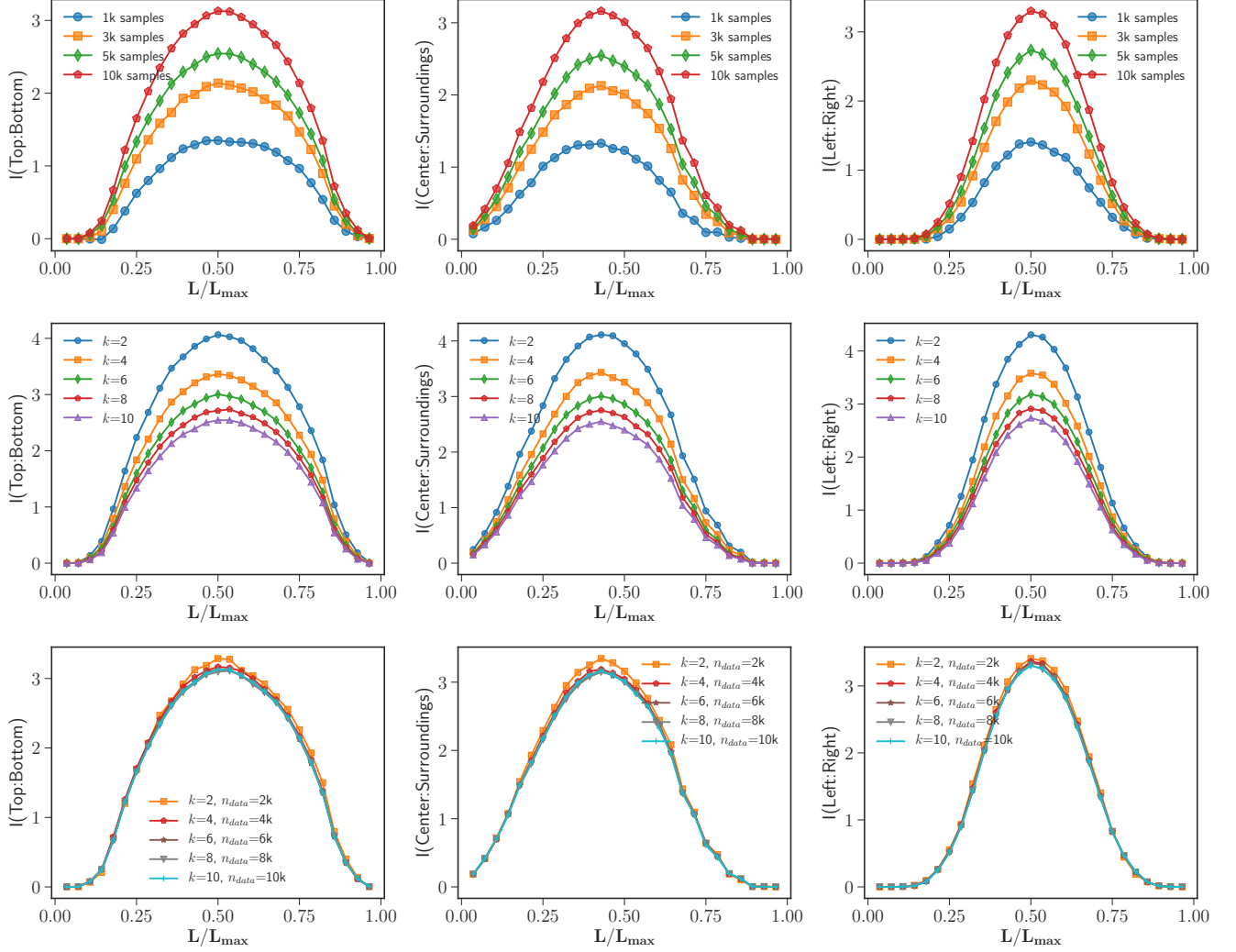


FIG. A.1. Details of the kNN estimation of MI in the MNIST data set. Top row, from Left to Right: Estimated $I(\text{left} : \text{right})$, $I(\text{center} : \text{surroundings})$, $I(\text{top} : \text{bottom})$ with $k = 10$ for 1k, 3k, 5k, 10k samples. Second row, from Left to Right: Estimated $I(\text{left} : \text{right})$, $I(\text{center} : \text{surroundings})$, $I(\text{top} : \text{bottom})$ with 5k samples and $k = 2, 4, 6, 8, 10$. The kNN estimation depends on the parameters k and the number of samples we use. Bottom row: Estimated $I(L : R)$, $I(C : S)$, $I(U : D)$ with $k \propto n_{\text{data}}$. For $k \propto n_{\text{data}}$, all curves collapse and we obtained a universal estimation.

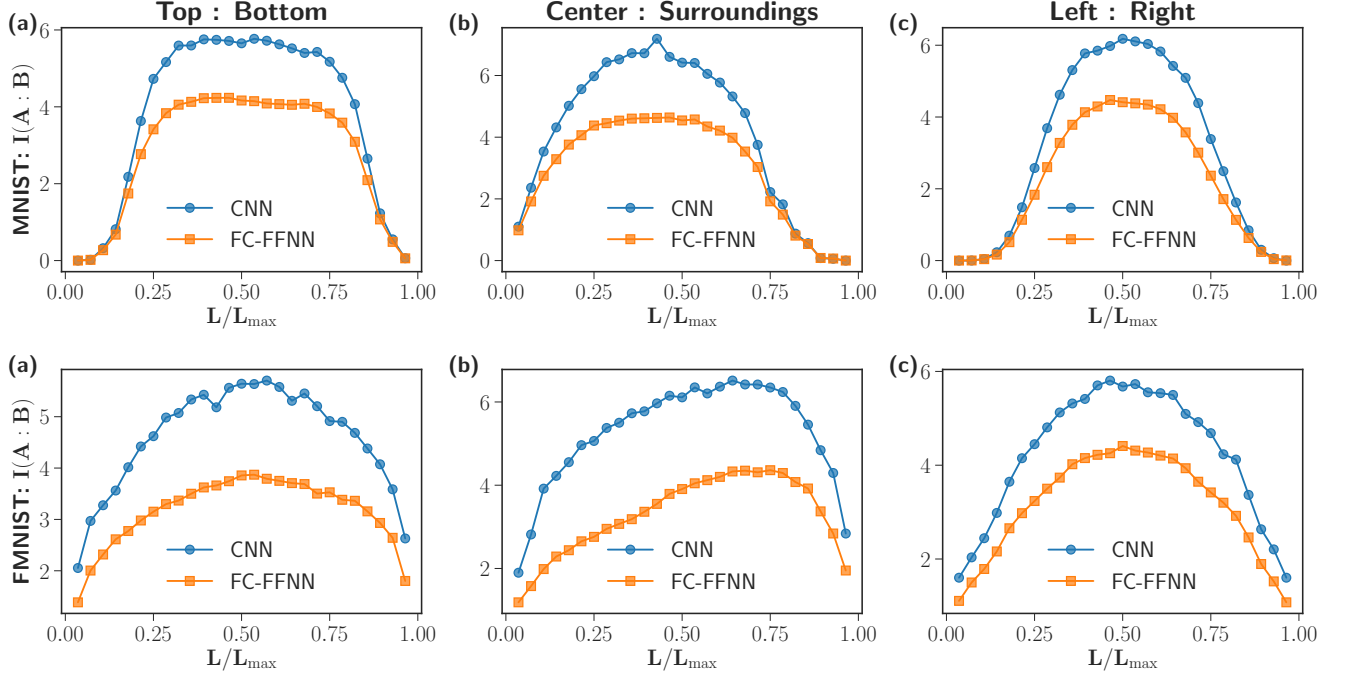


FIG. B.2. Details of the MINE estimation of MI in the MNIST and FashionMNIST data set. Top row: $I(L : R)$, $I(C : S)$, $I(T : B)$ with T_θ as multilayer convolutional neural network (CNN); Bottom row: $I(L : R)$, $I(C : S)$, $I(T : B)$ with T_θ as multilayer feed-forward fully connected neural networks (FFNN). We find that CNNs outperforms FFNNs.